Review

Imaging of the lamina cribrosa and its role in glaucoma: a review

Nicholas YQ Tan MA BMBCh,[1] Victor Koh MMed(Oph),[1,2] Michaël JA Girard PhD[1,3] and Ching-Yu Cheng MD PhD[1,4,5] iD

[1]Singapore Eye Research Institute, Singapore National Eye Centre, [2]Department of Ophthalmology, National University Hospital, [3]Department of Biomedical Engineering, National University of Singapore, [4]Ophthalmology and Visual Sciences Academic Clinical Program and Centre for Quantitative Medicine, Duke-NUS Medical School, and [5]Department of Ophthalmology, Yong Loo Lin School of Medicine, National University of Singapore, Singapore

ABSTRACT

The lamina cribrosa of the optic nerve head serves two contrasting roles; it must be porous to allow retinal ganglion cell axons to pass through, and yet at the same time, it must also provide adequate structural support to withstand the stresses and strains across it. Improvements in imaging such as optical coherence tomography image capture and image processing have allowed detailed *in vivo* studies of lamina cribrosa macro- and micro-architectural characteristics. This has aided our understanding of the optic nerve head as a complex biomechanical structure. In this review, we first aim to frame the biomechanical considerations of lamina cribrosa in a clinical context; in doing so, we also explore the concept of the translaminar pressure difference. Second, we aim to highlight the technological advances in imaging the lamina cribrosa and its accompanying clinical implications, and future directions in this quickly progressing field.

Key words: glaucoma, imaging, lamina cribrosa, optical coherence tomography, translaminar pressure difference.

INTRODUCTION

The lamina cribrosa (LC) is a reticulated, sieve-like structure that fills the posterior scleral foramen, which unmyelinated retinal ganglion cell (RGC) axons pass through before converging as the optic nerve (ON). The LC has long been identified as the main site of RGC axonal injury[1,2] and hence anatomically important in the pathogenesis of glaucoma. In recent years there has been renewed interest in studying this structure within a biomechanical framework. Part of the reason for this is that only with recent advances in optical coherence tomography (OCT) imaging has it been possible to study the LC in greater detail *in vivo*. Without OCT, pre-laminar neuroretinal tissue obscures the view of the LC on ophthalmoscopy or other modalities of imaging.

The purpose of this review was therefore two-fold. First, we aimed to explore why the LC as a biomechanical structure is of worthwhile study in glaucoma. Second, we aimed to highlight common techniques to image the LC *in vivo*, their clinical relevance, and future directions in this quickly progressing field.

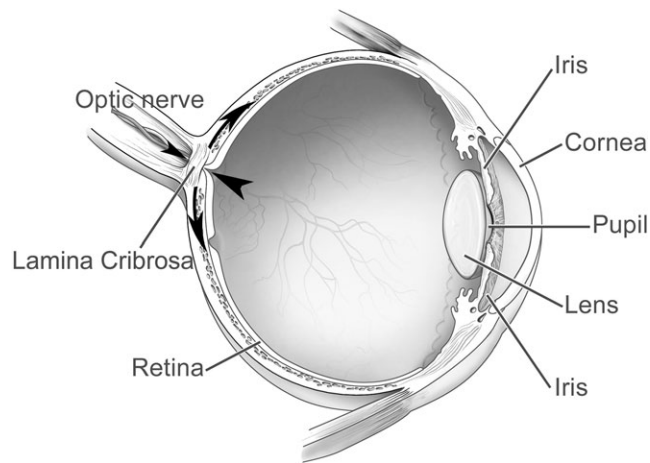## THE TRANSLAMINAR PRESSURE DIFFERENCE

The key to understanding the role of the LC in glaucoma comes from its anatomical location. The LC is situated between two differentially pressurized compartments, which the optic nerve head (ONH) is exposed to (Fig. 1).[3,4] Neural tissue pressure anterior to the LC is determined by the intraocular pressure (IOP), while neural tissue pressure posterior to the LC is determined by the cerebrospinal fluid (CSF) pressure (CSFP) in the subarachnoid space.

■ **Correspondence:** A/Prof Ching-Yu Cheng, Singapore Eye Research Institute, The Academia, 20 College Road, Discovery Tower, Level 6, Singapore 169856. Email: chingyu.cheng@duke-nus.edu.sg

Figure 1. A cross-sectional diagram of the eye illustrating the stresses across the lamina cribrosa. The difference between intraocular pressure (large arrowhead) and retrobulbar cerebrospinal fluid pressure (small arrowhead) results in the translaminar pressure gradient that stresses the lamina cribrosa in the anteroposterior axis. In addition, the intraocular pressure also generates a pressure load to the inner surface of the eye wall, creating an in-wall circumferential hoop stress (curved arrows).

The pressure difference across the LC is known as the translaminar pressure difference (TLPD = IOP - retrobulbar CSFP), and the gradient of pressure across the LC is known as the translaminar pressure gradient (TLPG = TLPD/LC thickness).

Classical theories of glaucoma focused mainly on the IOP. However, if the TLPD is ultimately is of pathological significance in glaucoma, considering IOP without taking into account the retrobulbar CSFP may only be considering half of the full equation.

The earliest evidence that CSFP may be involved in the pathogenesis of glaucoma was established by Yablonski *et al.* in an animal model.[5] In their experiments conducted on cats, the CSFP was lowered to −4 mmHg, and one eye was cannulated with the IOP being lowered to 0 mmHg, while the fellow eye was unchanged and remained normotensive. Subsequently, the normotensive eye developed an optic neuropathy with increased cup–disc ratio and posterior displacement of the LC, consistent with glaucoma, while the hypotensive eye did not. Further groundwork was laid by Morgan *et al.,* using a canine model in which the IOP and the retrolaminar tissue pressure were measured to derive the TPLG, and the IOP and CSFP were monitored and controlled.[3,6] It was found that at physiological pressures, the CSFP was the main determinant of the retrolaminar tissue pressure, and the effect of altering the CSFP was biomechanically comparable to altering the IOP. They thus concluded that individuals with low CSFP may have a higher TLPG, which could influence the development of

glaucoma.[3] Support for this theory came from two large retrospective studies by Berdahl *et al.* They found the mean CSFP was significantly lower, and the TLPD significantly higher, in patients with primary open angle glaucoma (POAG) or normal tension glaucoma (NTG), compared to non-glaucomatous controls, whereas patients with ocular hypertension had higher CSFPs compared to controls.[7,8] A prospective study also showed similar results: lumbar CSFP was the lowest in NTG patients (9.5 ± 2.2 mmHg), followed by POAG patients (11.7 ± 2.7 mmHg) and then controls (12.9 ± 1.9 mmHg), with significant differences between all three groups.[9]

CHALLENGES IN MEASURING THE TRANSLAMINAR PRESSURE DIFFERENCE

Although there is convincing evidence to suggest that CSFP may indeed be lower in patients with glaucoma compared to those without, it is impractical to measure CSFP routinely in glaucoma follow-up appointments, as is done for IOP. Lumbar puncture is invasive and fraught with potentially life-threatening complications.[10] On the other hand, non-invasive methods of measuring CSFP are unreliable.[11]

A further consideration in extrapolating the results of clinical studies that relied on lumbar puncture as a means of determining CSFP is that lumbar CSFP may not necessarily be a reliable proxy measurement of the retrobulbar CSFP. With an open CSF pathway throughout the spine, brain, and ON, lumbar and ventricular CSFP may be expected to be closely related to retrobulbar CSFP. However, the subarachnoid layer of the human ON is not a homogeneous chamber filled with CSF, but instead contains a variety of trabeculae, septa, and stout pillars that divide the subarachnoid space (SAS) and may impede CSF flow.[12] Computed tomography (CT) cisternography has also shown a relative stasis of CSF flow along the ON in eyes with NTG, but not in controls.[13] Further evidence for an 'ON compartment syndrome', where there is segregation of CSF between the intracranial and ON SAS, has also been demonstrated in patients with unilateral or highly asymmetrical optic disc swelling from various causes such as intracranial hypertension, cerebral haemorrhage and optic nerve sheath meningioma. By measuring the concentrations of a brain-derived protein lipocalin-like prostaglandin D-synthase that should expectedly be distributed homogenously throughout all the CSF, it was found that there was a concentration gradient between the CSF in the spine and CSF in the SAS of the ON, suggesting different CSF dynamics within two separate but interlinked compartments.[14]

The idea of compartmentation surrounding the ON helps explain how patients with intracranial hypertension may have unilateral or asymmetric papilledema.[15,16] Granted the assumption that low CSFP may result in glaucoma, it also explains how glaucoma may not infrequently be unilateral or asymmetric.[17,18] However, the compartmentation of the ON CSF may be difficult to detect clinically. To this end, imaging with CT or magnetic resonance imaging (MRI) has been attempted, although results have been inconsistent. Using CT or MRI, the ON sheath diameter in NTG has been shown to be reduced in some studies,[19] but widened in other studies.[20,21] Furthermore, ON sheath diameters have not always been shown to be significantly correlated with lumbar CSFPs[21]; this could be due to the biomechanical properties of ON sheath tissues that are likely vary across individuals and that have not been well studied.

Although there are no reliable ways of determining retrobulbar CSFP in routine clinical practice, it should be remembered that it is not the absolute retrobulbar CSFP that is of final importance in glaucoma, but rather the pressures in the retrobulbar and intraocular spaces relative to each other, that is, the TLPD. This is where imaging of the LC comes in. In the following sections, we will first explore techniques of imaging the LC *in vivo*, followed by a discussion of how imaging can be used to better understand the biomechanical behaviour and environment of the LC.

TECHNIQUES OF IMAGING THE LAMINA CRIBROSA *IN VIVO*

The most basic method of imaging the LC is through optic disc photography (Fig. 2). Although the mid- to far-periphery of the LC is obscured by pre-laminar neuroretinal tissue, part of the anterior surface of the LC may be viewed through the thinner, semi-transparent central pre-laminar tissue. A crude qualitative 2D assessment of the anterior LC using disc photography does not allow for detailed structural descriptions of the LC morphometry, but is sufficient for identifying gross LC features such as the presence of LC pores, the number and shape of which are thought to be associated with glaucoma.[22,23]

Confocal scanning laser ophthalmoscopy (CSLO) may be used to image the ONH *in vivo*. It is a microscopic imaging technique that rapidly scans the area of interest with a near-infrared diode laser beam in a raster fashion. In doing so, a 2D image of the ONH can be built up as an array of pixels, with a series of 2D CSLO images obtained at successive planes of depth in the tissue, these can be used to construct a 3D image. CSLO can therefore provide *en face* images of the anterior laminar surface, although it is

Figure 2. An optic disc photograph of a glaucomatous eye. Lamina cribrosa pores are readily visible, and an optic disc haemorrhage (arrow) is also present at the inferotemporal disc border.

limited by poor resolution and depth penetrance. For this reason, earlier imaging studies of the LC using CSLO were only able to investigate gross LC morphology (such as the area of the LC, or the number and size of pores), rather than detailed structural assessment.[24,25] Further improvement to CSLO came with the advent of adaptive optics (AO), which uses a wavefront sensor to measure ocular aberrations, and a deformable mirror or a spatial light modulator to compensate for the measured aberrations to improve the lateral resolution of the images. Nevertheless, AO-CSLO studies have been limited mainly to the study of LC pore morphology.[26–28]

On the other hand, advances in OCT image acquisition and image processing have enabled dramatic improvements in visualizing the LC in greater detail. The earlier modality of OCT imaging, that is time-domain (TD)-OCT, had a limited ability to image the LC, because of a depth-dependent decrease in sensitivity and scattering of light by pigment and blood. Furthermore, as TD-OCT employs approximately 400 A-scans per second using 6 radial slices oriented 30° apart, axial resolution of the scan may be limited to approximately 10 μm.[29] However, with spectral-domain (SD)-OCT, which has largely replaced TD-OCT, axial resolution may be as good as up to 2 μm.[30] SD-OCT detects the backreflected light simultaneously by measuring the interference spectrum using an interferometer with a high-speed spectrometer – this enables higher scan rates of up to 80 000 A scans per second. More recently, a

third-generation OCT modality has been introduced called swept-source (SS)-OCT.[31] In SS-OCT, a short cavity swept laser with a tunable wavelength of operation is used instead of the diode laser used in SD-OCT. With a longer wavelength (1050 nm in SS-OCT *vs.* 840 nm in SD-OCT), tissue penetrance and visibility of deeper structures is improved. Additionally, because SS-OCT does not require averaging of multiple B-scans to visualize the deep tissues, it allows 3D raster scanning with excellent sampling density, enabling clearer observation of the 3D structure of the optic disc.

However, SD-OCT or SS-OCT on their own are of limited use in imaging aspects of the LC located deeply within the ONH because of the attenuated signal strength at greater depths. Fortunately, recent improvements in OCT hardware (e.g. enhanced depth imaging [EDI]) and OCT light-attenuation correction software (e.g. adaptive compensation [AC]) have significantly improved the visibility of the LC.[32–35] EDI OCT was originally developed to better image the posteriorly located choroid,[32] although it has also been adopted to provide detailed cross-sectional images of the LC. In EDI OCT, the OCT device is pushed close enough to the eye to create an inverted image near the top of the display. This has the effect of delivering the most tightly focused portion of the illumination at the level of deeper structures such as the choroid (or LC). Because these deeper structures are placed closer to the zero delay, the sensitivity of imaging of those structures is enhanced.[32] EDI may be used on SD-OCT or SS-OCT with or without AC (Fig. 3). AC is a post-processing technique that was developed to remove blood vessel shadows, enhance tissue contrast and reduce noise over-amplification.[33–35] In AC, a threshold exponent is used to remove the effects of noise over-amplification at high depth, thus facilitating posterior LC surface detection. This has been shown to improve the visibility of the anterior LC surface, insertion points and focal LC defects, as well help in identifying the posterior LC surface in subsets of patients. In a study of three different commercially available SD- and SS-OCT devices, AC was found to be superior to EDI in improving LC visibility, although the best anterior LC visibility grades overall were achieved with the Cirrus SD-OCT machine using both EDI and AC.[35]

With advances in OCT technology, OCT has gained popularity as the imaging modality of choice in capturing the macro-architectural features of the LC (e.g. its insertion points, anterior surface shape and overall thickness). Of late, the 3D microarchitecture of the LC has also been reliably studied with OCT (with and without AO) as well.[36–38] This has been made possible not only by the improved quality of the images, but also by the development of
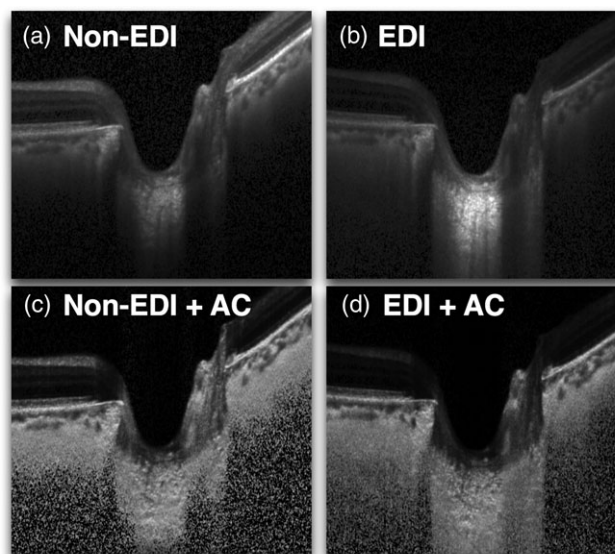
Figure 3. Imaging of the optic nerve head using spectal-domain optical coherence tomography (SD-OCT; Spectralis, Heidelberg Engineering GmbH, Heidelberg, Germany). (a) SD-OCT, without enhanced depth imaging (EDI). (b) SD-OCT with EDI. (c) SD-OCT with adaptive compensation (AC). (d) SD-OCT with EDI and AC.

automated techniques capable of segmenting and analysing individual LC beams and pores. The potential usefulness of being able to quantitatively assess the micro-architectural LC characteristics (e.g. total connective tissue volume, beam thickness and pore diameter) *in vivo* is hard to overstate, as such insights were previously only available through postmortem histological studies. For instance, in an experimental glaucoma model in monkeys, alterations to the LC total connective tissue volume were shown to occur in the early stages of glaucomatous damage,[39] before the development of any changes to the character of the LC microarchitecture (e.g. beam orientation and anisotropy), which from other studies is known to occur.[40,41] Whether such early microstructural changes may be replicable in humans, or useful in identifying pre-perimetric glaucoma are some of the potential new areas of enquiry facilitated by advances in OCT technology.

THE LAMINA CRIBROSA AS A BIOMECHANICAL STRUCTURE

Through histological studies, the morphology of the LC has been well-characterized as a three-dimensional, reticulated, multi-lamellar sieve-like structure of load-bearing trabeculae that provides structural and nutritional support (from the laminar capillaries within the laminar beams) to the unmyelinated RGC axons as they pass through it.[42–44] Within the laminar beams, elastin fibres and type I

and III collagen fibrils are longitudinally arranged within a proteoglycan matrix.[45–48] Where the laminar beams insert into the scleral canal, elastin fibres from the beams join a ring of collagen and elastin fibres along the border of the scleral wall.[49–52] Various aspects of the extracellular matrix of the LC and peripapillary sclera are thought to resist tensile, compressive and shear stresses in an interconnected and complex manner.[50,53,54] This network of connective tissues strengthens the eyeball at what would otherwise be a weak spot,[55,56] where the porous LC is only a third of the thickness of sclera at the peri-optic nerve region.[57] Mechanical stress may thus be concentrated at the LC insertion sites due to a mismatch in biomechanical properties between the peripapillary sclera and the weaker LC.

According to the biomechanical theory of glaucoma, interactions of IOP and retrobulbar CSFP may induce mechanical stress (a measure of internal tissue forces), and mechanical strain (the gold-standard measure for deformation) within the ONH tissues by at least two mechanisms: first, by the TLPG across the anterior and posterior surfaces of the LC (albeit a smaller force); and second, by an in-wall 'hoop' stress that acts in a circumferential manner (Fig. 1).[58]

It is well known that IOP-related stresses may induce extracellular matrix remodelling and chronic changes to the ONH that results in the typical excavated or cupped appearance of a glaucomatous optic disc,[59–63] which is for the most part irreversible even after the reduction of IOP. Through experimental glaucoma models in monkeys, it has been established that early glaucomatous changes to the ONH include posterior bowing of the lamina and peripapillary sclera that is accompanied by scleral canal expansion, thickening of the LC, and outward migration of the laminar insertion from the sclera into the pia mater.[64–67] Thus, when the IOP is chronically high as it is in glaucoma (the TLPD is high), the ONH is excavated and the LC posteriorly displaced.[59,68] On the other hand, in intracranial hypertension where the CSFP is high (and hence the TLPD is low), there is papilloedema and the OHN is swollen and the LC anteriorly displaced.[68–70] Interestingly, in ocular hypotony (where the TLPD is also low), optic disc swelling may also be present.[71] Thus, it may seem intuitive that for a given increase in the IOP (or TLPD), the LC should deform posteriorly, and vice versa.

Accordingly, there have been several experimental (ex vivo and in vivo, in animals as well as humans) and computational studies investigating the response of the LC with dynamic changes in the IOP. Most ex vivo studies of post-mortem human[72–74] or animal[64] eyes have showed that the LC deformed posteriorly with IOP elevation. Although some

in vivo studies using OCT have also supported this finding,[75–77] other OCT studies have found that the movement of the LC may be either posterior or anterior following an increase in IOP,[78,79] which was also predicted using computational modelling.[80–82] The observation of the bi-directional displacement of the LC may be explained by considering the biomechanics of not just the LC, but also the peripapillary sclera to which it is anchored to. With an increase in the IOP, the hydrostatic forces across the TLPG may tend to deform the LC posteriorly; however, the circumferentially acting hoop stress tends to expand the scleral canal, draw the LC taut and deform it anteriorly. Whether the posterior or anterior forces prevails in a particular eye depends on the specific mechanical and geometrical properties of its LC-peripapillary scleral complex, such as the thickness and position of the LC, and the structural stiffness of the LC and the peripapillary sclera.[58,81–83] The IOP-related stresses and strains on the LC are therefore very complicated and may be not adequately described by observing its deformation in just one dimension (e.g. anterior/posterior displacement). In a three-dimensional model, it was recently shown by Tun et al. that dynamic elevations of IOP significantly altered the anterior LC shape in a complex non-linear pattern, with the overall movement of the LC in different eyes being sometimes posterior and sometimes anterior.[79] Acute changes in the LC structure as a result of dynamic alterations in IOP (as in the above-mentioned experiments) should therefore not be considered as equivalent to the chronic deformations (or remodelling) of the LC secondary to long-standing changes in the IOP (e.g. in untreated glaucoma).

STRUCTURAL PARAMETERS OF THE LAMINA CRIBROSA ON OPTICAL COHERENCE TOMOGRAPHY

A few macro-structural parameters, however, have been commonly used to describe both the acute and chronic deformations/changes to LC. Such parameters include the anterior LC depth (LCD),[84–86] LC curvature (LCC),[85–88] and the index of the anterior LC 3D morphology.[88] LCD is often defined as the maximum or mean vertical distance from the anterior LC surface to the reference plane of Bruch's membrane opening (BMO). Multiple OCT studies have demonstrated that the LCD is greater in eyes with glaucoma compared to healthy eyes.[84–86] Additionally, the LCD was shown to correlate with the TLPD and TLPG.[89] When the IOP in glaucomatous eyes was lowered after the introduction of medical therapy,[90] or after glaucoma filtration surgery,[91,92] a mean reduction in the anterior LCD was noted. In prospective studies of glaucoma patients, greater

LCD was also associated with greater visual field progression[93] and faster rates of retinal nerve fibre layer (RNFL) thinning.[94]
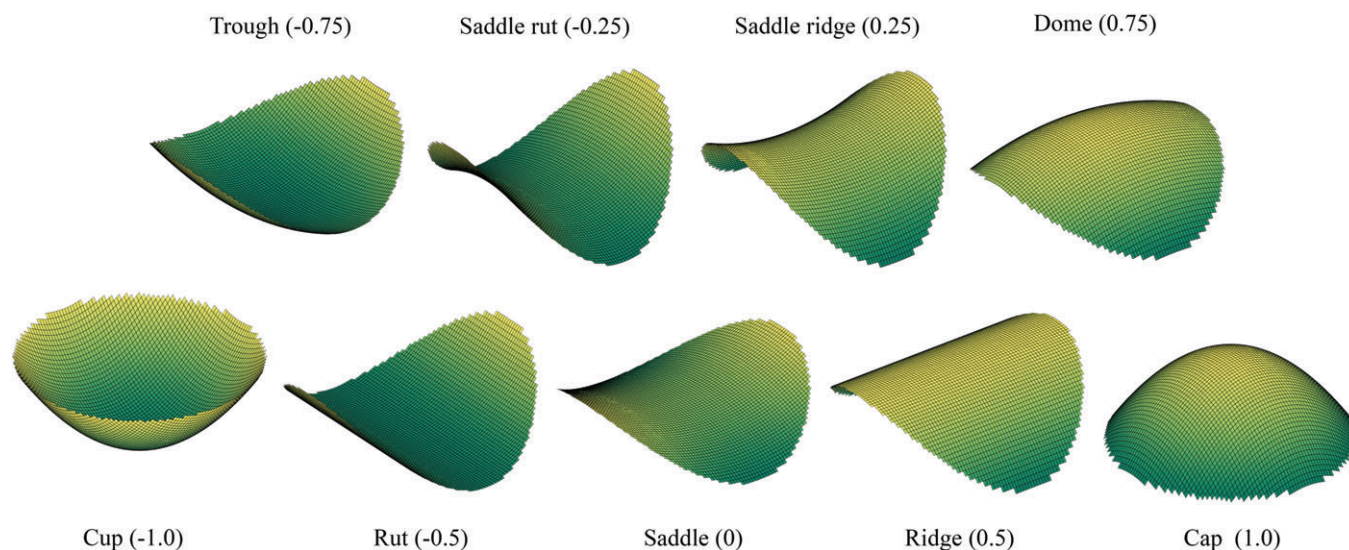
However, results with LCD have not always been consistent. For instance, although Reis *et al.*[91] and Lee *et al.*[92] found reduction in the LCD after glaucoma surgery, Girard *et al.*, using an OCT-based 3D tracking algorithm, demonstrated that although 3D-strain was reduced after IOP lowering surgery, the LC could displaced posteriorly, anteriorly or not at all.[95] Furthermore, although 3D-strain was reduced when IOP was lowered, this was not significantly correlated with the amount of IOP reduction.[95] This may be because the strain on the ONH is dependent on not just the IOP, but also the CSFP and the biomechanical properties of the LC and the parapapillary scleral. Thus, the effect of any magnitude of IOP reduction must also consider these other factors. For illustrative purposes, consider two eyes *A* and *B*. *A* has IOP of 40 mmHg, CSFP of 5 mmHg, LC thickness of 0.3 mm and TLPG of 116.7 mmHg/mm ([40−5]/0.3 = 116.7); with reduction of IOP to 20 (50% reduction), the TLPG drops to 50 mmHg/mm (57.1% reduction). *B* has IOP of 40 mmHg, CSFP of 15 mmHg, LC thickness of 0.5 mm and TLPG of 50 mmHg/mm; with reduction of IOP to 20 mmHg (50% reduction), the TLPG drops to 10 mmHg/mm (80% reduction). Thus, we see that for two eyes with the same starting pressures, a reduction of IOP by the same magnitude may have strikingly different resultant TLPGs.

An additional limitation of LCD as an ONH biomechanical-parameter is that it requires the use of a reference plane. This is problematic because using the BMO as a reference plane also includes choroidal thickness in the measurement of LCD. Thus, LCD may be altered by choroidal thickness, which may vary with age and other non-glaucomatous pathology.[96,97] The alternative assignment of the anterior sclera as a reference plane for LCD, as has been done in other studies,[98] is also not ideal as the peripapillary sclera may deform alongside the LC secondary to changes in IOP.[81] As such, the LC curvature, which does not require the use of a reference plane, has been proposed as an alternative structural parameter that is also related to glaucoma.

It is postulated that the extent of posterior bowing of the LC (i.e. greater posterior LCC) may indicate the amount of IOP-related strain over the ONH. As evidence for this, various clinical studies have demonstrated that: (i) posterior bowing of the LC was greater in glaucomatous compared to healthy eyes[87,99]; (ii) LCC was associated with IOP[85,100]; (iii) LCC was reduced after trabeculectomy[100]; and (iv) LCC had greater discriminating capability between POAG and healthy eyes than LCD.[85] However, LCC as an ONH biomechanical-parameter is not without its own shortcomings. For instance, different methods of measuring the posterior bowing of the LC exist,[85,87,88] with no clear consensus on which may be most appropriate, or how each measurement relates to the others. Furthermore, the measured curvature of the LC would depend on which meridian is chosen for analysis. As a form of 2D analysis, this naturally does not capture the full complexity of the LC as a 3D structure.

To address some of these limitations, the LC global shape index (LC-GSI) was developed (Fig. 4).[88] The LC-GSI is a number from the range of −1 (corresponding to a spherical cup) to +1

Figure 4. Illustration of the lamina cribrosa global shape index (LC-GSI), which is a number from the range of −1 (corresponding to a spherical cup) to +1 (corresponding to a spherical cap) that describes the local surface shape of the anterior LC; nine categories are shown, with the LC-GSI in parentheses: cup, trough, rut, saddle rut, saddle, saddle ridge, ridge, dome and cap.

(corresponding to a spherical cap) that describes the overall geometrical shape of the anterior LC surface from a 3D ONH reconstruction, without the need of a reference plane. The LC-GSI was found to be significantly associated with VCDR and minimum rim width,[88] both of which are structural parameters related to glaucoma.[101] Further utility of the LC-GSI was demonstrated in another study where both healthy and glaucomatous eyes were subject to acute IOP elevations from an ophthalmodynamometer.[79] In that study, although complex non-linear dynamic changes to the anterior LC surface could be detected using the LC-GSI, LCD was not changed significantly overall. Additionally, in our own data, we have found the LC-GSI to be significantly associated with severity of glaucoma. As other commonly reported OCT parameters of the ONH are concerned with pre-laminar changes only (e.g. neuroretinal rim thinning), the complementary usage of LC-GSI as a LC-specific OCT parameter may be potentially advantageous in the assessment and monitoring of glaucoma.

The LC-GSI, LCD and LCC, however, are parameters related only to the anterior surface of the LC. It does not take into account the posterior surface of the LC or its thickness. Although there has been evidence to suggest that LC thinning is associated with glaucoma[94,102] (the LC thickens initially,[63,67] but may remodel and thin out with progression of disease[103]; alternatively, a thinner LC may be a risk factor that amplifies the TPLG), the posterior LC surface is notoriously hard to consistently image well with currently available imaging modalities.[35]

LAMINA CRIBROSA MICROARCHITECTURE AND FOCAL DEFECTS ON OPTICAL COHERENCE TOMOGRAPHY

OCT imaging has also been used to identify other morphological characteristics of the LC, such focal LC defects (FLDs), and on a more minute level, changes to the laminar beam and pore structure.

Although focal defects to the LC have been inconsistently defined in the literature (it has been variably used to describe laminar holes or disinsertions,[104] laminar surface irregularities,[105] or pits or cavities in the LC[106]), evidence is accumulating that these changes may represent a structural feature of glaucomatous optic neuropathy. Multiple studies have shown that FLDs are more common in glaucomatous eyes.[105,107] Furthermore, spatial correspondence between focal RNFL defects and FLDs have also been suggested.[107] In a prospective study, FLDs were strongly associated with glaucomatous visual field progression.[108]

The occurrence of FLDs in glaucoma may also help explain the phenomenon of optic disc haemorrhages (Fig. 2). A number of recent OCT studies have demonstrated that disc haemorrhages are associated with FLDs.[109–112] In this schema, disc haemorrhages may be a consequence of local disruption of lamina beams and the rupture of its accompanying pre-laminar or laminar beam capillaries. However, it is the focal loss of the lamina beams, and hence the structural and metabolic support to RGC axons, that ultimately results in the RGC axonal loss characteristic of glaucoma. As support for this hypothesis, it has been found that both FLDs and optic disc haemorrhages are associated with each other, and also with localized RNFL loss.[105,107,113]

In more recent times, OCT has also been used to visualize the microarchitecture of the LC *in vivo*.[36–38] For instance, by this means, it has been demonstrated that in glaucoma, there is an increase in beam thickness, reduction in pore size, and increase in pore variability.[41] Whether this might be related to LC remodelling (thickening of laminar beams to distribute the increased stress), focal damage to the LC (causing some pores to drastically lose diameter, thus increasing the variability in pore diameter) or axonal loss (shrinking of pores consequent to axonal loss) is speculative due to the cross-sectional nature of the data.[41] However, the capability to detect and quantify such changes in beam and pore morphology offers exciting new avenues of enquiry.

OPTIC NERVE HEAD STRAIN FROM EYE MOVEMENTS

In much of the discussion thus far, strain on the ONH has been understood to come from two main sources, that is, the IOP and retrobulbar CSFP. However, it has lately been suggested that horizontal eye movements may act as a third loading mechanism on the ONH. Imaging modalities that include MRI and OCT have been valuable in studying this hypothesis.

MRI studies have demonstrated that eye movements are capable of generating large deformations within the ONH through the pulling action of the ON sheaths.[114,115] Using finite element modelling, it was estimated that these ONH deformations from eye movements were comparable to the effect of elevating the IOP by as much as 50 mmHg.[115] Separate OCT studies, which offer significantly better resolution compared to MRI, have also come to similar conclusions.[116–118] Using an OCT-based 3D tracking technology to quantitatively map *in vivo* LC deformations induced by eye movements, Wang *et al.* was able to demonstrate that the LC strains in adduction were large and comparable to those following a substantial IOP increase of 30 to 40 mmHg.[116] Suh *et al.* further reported that ONH deformations with graded horizontal ductions did not follow a simple linear

relationship, but rather, ONH deformations in adduction increased sharply after exceeding a threshold of 26°.[117] This is in agreement with the concept of ON sheath tethering the globe in adduction, which was estimated from MRI studies to occur in the range of 22° to 26°.[114] The implication these studies may have on our understanding of the pathogenesis of glaucoma is still uncertain.

CONCLUSION

In the 1950s, high IOP was thought to be virtually synonymous with glaucoma, where eyes with IOPs of 21 mmHg and above were considered to be glaucomatous, irrespective of structural or functional changes.[119] Although the recognition of entities such as NTG and ocular hypertension has helped to redefine our understanding of the role IOP plays in the pathogenesis of glaucoma, in clinical practice, the diagnosis and monitoring of glaucoma still remains very IOP-centric. It is our view that the pressure difference across the cornea (i.e. the IOP) is ultimately of less importance than the pressure difference across the LC (i.e. the TLPD), which is the main site of RGC axonal insult in glaucoma. However, it is not straightforward to accurately determine the mechanical strain across the LC (for instance, as induced by the TLPD). Furthermore, the response of the ONH to the TLPD (i.e. the susceptibility of the ONH to pressure-related glaucomatous optic neuropathy) is also dependent on biomechanical properties of the LC and peri-papillary scleral complex. Thus, a better understanding of ONH biomechanics is required to realize the potential clinical applications of measuring LC mechanical strains *in vivo*. To this end, recent advances in imaging modalities that allow better morphological characterization of the LC are good first steps in the right direction.

Nevertheless, our understanding of the biomechanical behaviour, microstructure and morphology of the LC *in vivo* is still in its infancy. There is a pressing need to validate and confirm existing measurements, and to better understand all the loads acting on the ONH (such as IOP, retrobulbar CSFP and optic nerve traction). Improvements in OCT hardware, including AO,[36] swept source,[41] multiple wavelengths, phase-sensitive technology,[120] low-coherence interferometry,[121] μ-imaging[122] and image processing techniques such as AC,[33,34] are likely to push the quality and availability of *in vivo* biomechanical, morphological and microstructural measurements to the next level.

REFERENCES

1. Quigley H, Anderson DR. The dynamics and location of axonal transport blockade by acute intraocular pressure elevation in primate optic nerve. *Invest Ophthalmol* 1976; **15**: 606–16.
2. Quigley HA, Addicks EM, Green WR, Maumenee AE. Optic nerve damage in human glaucoma. II. The site of injury and susceptibility to damage. *Arch Ophthalmol* 1981; **99**: 635–49.
3. Morgan WH *et al.* The influence of cerebrospinal fluid pressure on the lamina cribrosa tissue pressure gradient. *Invest Ophthalmol Vis Sci* 1995; **36**: 1163–72.
4. Jonas JB, Berenshtein E, Holbach L. Anatomic relationship between lamina Cribrosa, intraocular space, and cerebrospinal fluid space. *Invest Ophthalmol Vis Sci* 2003; **44**: 5189–95.
5. Yablonski ME, Ritch R, K. P. Effect of decreased intracranial-pressure on optic disk. *Invest Ophthalmol Vis Sci* 1979; **18**: 165.
6. Morgan WH *et al.* The correlation between cerebrospinal fluid pressure and retrolaminar tissue pressure. *Invest Ophthalmol Vis Sci* 1998; **39**: 1419–28.
7. Berdahl JP, Allingham RR, Johnson DH. Cerebrospinal fluid pressure is decreased in primary open-angle glaucoma. *Ophthalmology* 2008; **115**: 763–8.
8. Berdahl JP, Fautsch MP, Stinnett SS, Allingham RR. Intracranial pressure in primary open angle glaucoma, normal tension glaucoma, and ocular hypertension: a case-control study. *Invest Ophthalmol Vis Sci* 2008; **49**: 5412–8.
9. Ren R, Jonas JB, Tian G *et al.* Cerebrospinal fluid pressure in glaucoma. A prospective study. *Ophthalmology* 2010; **117**: 259–66.
10. Dripps RD, Vandam LD. Hazards of lumbar puncture. *JAMA* 1951; **147**: 1118–21.
11. Khan MN, Shallwani H, Khan MU, Shamim MS. Noninvasive monitoring intracranial pressure - a review of available modalities. *Surg Neurol Int* 2017; **8**: 51.
12. Killer HE, Laeng HR, Flammer J, Groscurth P. Architecture of arachnoid trabeculae, pillars, and septa in the subarachnoid space of the human optic nerve: anatomy and clinical considerations. *Br J Ophthalmol* 2003; **87**: 777–81.
13. Killer HE, Miller NR, Flammer J *et al.* Cerebrospinal fluid exchange in the optic nerve in normal-tension glaucoma. *Br J Ophthalmol* 2012; **96**: 544–8.
14. Killer HE, Jaggi GP, Flammer J, Miller NR, Huber AR. The optic nerve: a new window into cerebrospinal fluid composition? *Brain* 2006; **129**: 1027–30.
15. Strominger MB, Weiss GB, Mehler MF. Asymptomatic unilateral papilledema in pseudotumor cerebri. *J Clin Neuroophthalmol* 1992; **12**: 238–41.
16. Huna-Baron R, Landau K, Rosenberg M, Warren FA, Kupersmith MJ. Unilateral swollen disc due to increased intracranial pressure. *Neurology* 2001; **56**: 1588–90.
17. Frequency of asymmetric visual field defects in normal-tension and high-tension glaucoma1. *Ophthalmology* 1998; **105**: 988–91.
18. Kim C, Kim T-W. Comparison of risk factors for bilateral and unilateral eye involvement in normal-tension glaucoma. *Invest Ophthalmol Vis Sci* 2009; **50**: 1215.

19. Wang N et al. Orbital cerebrospinal fluid space in glaucoma: the Beijing intracranial and intraocular pressure (iCOP) study. Ophthalmology 2012; 119: 2065–73.

20. Jaggi GP, Miller NR, Flammer J, Weinreb RN, Remonda L, Killer HE. Optic nerve sheath diameter in normal-tension glaucoma patients. Br J Ophthalmol 2012; 96: 53–6.

21. Pircher A, Montali M, Berberat J, Remonda L, Killer HE. Relationship between the optic nerve sheath diameter and lumbar cerebrospinal fluid pressure in patients with normal tension glaucoma. Eye 2017; 31: 1365–72.

22. Susanna R. The lamina cribrosa and visual field defects in open-angle glaucoma. Can J Ophthalmol 1983; 18: 124–6.

23. Miller KM, Quigley HA. The clinical appearance of the lamina cribrosa as a function of the extent of glaucomatous optic nerve damage. Ophthalmology 1988; 95: 135–8.

24. Fontana L, Bhandari A, Fitzke FW, Hitchings RA. In vivo morphometry of the lamina cribrosa and its relation to visual field loss in glaucoma. Curr Eye Res 1998; 17: 363–9.

25. Bhandari A, Fontana L, Fitzke FW, Hitchings RA. Quantitative analysis of the lamina cribrosa in vivo using a scanning laser opthalmoscope. Curr Eye Res 1997; 16: 1–8.

26. Vilupuru AS, Rangaswamy NV, Frishman LJ, Smith III EL, Harwerth RS, Roorda A. Adaptive optics scanning laser ophthalmoscopy for in vivo imaging of lamina cribrosa. J Opt Soc Am A 2007; 24: 1417.

27. Ivers KM, Li C, Patel N et al. Reproducibility of measuring lamina Cribrosa pore geometry in human and nonhuman primates with in vivo adaptive optics imaging. Invest Ophthalmol Vis Sci 2011; 52: 5473–80.

28. Akagi T, Hangai M, Takayama K, Nonaka A, Ooto S, Yoshimura N. In vivo imaging of lamina Cribrosa pores by adaptive optics scanning laser ophthalmoscopy. Invest Ophthalmol Vis Sci 2012; 53: 4111.

29. Sigal IA, Wang B, Strouthidis NG, Akagi T, Girard MJA. Recent advances in OCT imaging of the lamina cribrosa. Br J Ophthalmol 2014; 98: ii34–9.

30. Wojtkowski M, Srinivasan VJ, Ko TH, Fujimoto JG, Kowalczyk A, Duker JS. Ultrahigh-resolution, high-speed, Fourier domain optical coherence tomography and methods for dispersion compensation. Opt Express 2004; 12: 2404–22.

31. Potsaid B, Baumann B, Huang D et al. Ultrahigh speed 1050nm swept source/Fourier domain OCT retinal and anterior segment imaging at 100,000 to 400,000 axial scans per second. Opt Express 2010; 18: 20029–48.

32. Spaide RF, Koizumi H, Pozzoni MC, Pozonni MC. Enhanced depth imaging spectral-domain optical coherence tomography. Am J Ophthalmol 2008; 146: 496–500.

33. Girard MJA, Strouthidis NG, Ethier CR, Mari JM. Shadow removal and contrast enhancement in optical coherence tomography images of the human optic nerve head. Invest Ophthalmol Vis Sci 2011; 52: 7738–48.

34. Mari JM, Strouthidis NG, Park SC, Girard MJA. Enhancement of lamina cribrosa visibility in optical coherence tomography images using adaptive compensation. Invest Ophthalmol Vis Sci 2013; 54: 2238–47.

35. Girard MJA, Tun TA, Husain R et al. Lamina Cribrosa visibility using optical coherence tomography: comparison of devices and effects of image enhancement techniques. Invest Ophthalmol Vis Sci 2015; 56: 865–74.

36. Nadler Z, Wang B, Wollstein G et al. Automated lamina cribrosa microstructural segmentation in optical coherence tomography scans of healthy and glaucomatous eyes. Biomed Opt Express 2013; 4: 2596–608.

37. Nadler Z, Wang B, Wollstein G et al. Repeatability of in vivo 3D lamina cribrosa microarchitecture using adaptive optics spectral domain optical coherence tomography. Biomed Opt Express 2014; 5: 1114–23.

38. Nadler Z, Wang B, Schuman JS et al. In vivo three-dimensional characterization of the healthy human lamina Cribrosa with adaptive optics spectral-domain optical coherence tomography. Invest Ophthalmol Vis Sci 2014; 55: 6459–66.

39. Roberts MD, Grau V, Grimm J et al. Remodeling of the connective tissue microarchitecture of the lamina Cribrosa in early experimental glaucoma. Invest Ophthalmol Vis Sci 2009; 50: 681–90.

40. Reynaud J, Lockwood H, Gardiner SK, Williams G, Yang H, Burgoyne CF. Lamina Cribrosa microarchitecture in monkey early experimental glaucoma: global change. Invest Ophthalmol Vis Sci 2016; 57: 3451–69.

41. Wang B, Nevins JE, Nadler Z et al. In vivo lamina Cribrosa micro-architecture in healthy and glaucomatous eyes as assessed by optical coherence tomography. Invest Ophthalmol Vis Sci 2013; 54: 8270–4.

42. Anderson DR. Ultrastructure of human and monkey lamina Cribrosa and optic nerve head. Arch Ophthalmol 1969; 82: 800–14.

43. Elkington AR, Inman CBE, Steart PV, Weller RO. The structure of the lamina cribrosa of the human eye: An immunocytochemical and electron microscopical study. Eye 1990; 4: 42–57.

44. Wilczek M. The lamina Cribrosa and its nature. Br J Ophthalmol 1947; 31: 551–65.

45. Hernandez MR, Luo XX, Igoe F, Neufeld AH. Extracellular matrix of the human lamina Cribrosa. Am J Ophthalmol 1987; 104: 567–76.

46. Morrison JC, Jerdan JA, L'Hernault NL, Quigley HA. The extracellular matrix composition of the monkey optic nerve head. Invest Ophthalmol Vis Sci 1988; 29: 1141–50.

47. Morrison JC, L'Hernault NL, Jerdan JA, Quigley HA. Ultrastructural location of extracellular matrix components in the optic nerve head. Arch Ophthalmol 1989; 107: 123–9.

48. Jan N-J, Grimm JL, Tran H et al. Polarization microscopy for characterizing fiber orientation of ocular tissues. Biomed Opt Express 2015; 6: 4705–18.

49. Quigley HA, Dorman-Pease ME, Brown AE. Quantitative study of collagen and elastin of the optic nerve head and sclera in human and experimental monkey glaucoma. Curr Eye Res 1991; 10: 877–88.

50. Zhang L, Albon J, Jones H *et al*. Collagen microstructural factors influencing optic nerve head biomechanics. *Invest Ophthalmol Vis Sci* 2015; **56**: 2031.

51. Albon J, Karwatowski WS, Easty DL, Sims TJ, Duance VC. Age related changes in the non-collagenous components of the extracellular matrix of the human lamina cribrosa. *Br J Ophthalmol* 2000; **84**: 311–7.

52. Pijanka JK, Coudrillier B, Ziegler K *et al*. Quantitative mapping of collagen fiber orientation in non-glaucoma and glaucoma posterior human Sclerae. *Invest Ophthalmol Vis Sci* 2012; **53**: 5258–70.

53. Zeimer R. Biomechanical properties of the optic nerve head. Optic Nerve in Glaucoma. Amsterdam: Kugler Publications, 1995; 107–21.

54. Hernandez M, Gong H. *Extracellular Matrix of the Trabecular Meshwork and Optic Nerve Head Glaucomas*. St. Louis: Mosby, 1996.

55. Von Graefe A. Ueber die Iridektomie bei Glaucom und uber den glaucomatosen process. *Albr Von Graefes Arch Klin Exp Ophthalmol* 1857; **3**: 456–555.

56. Tansley K. Comparison of the lamina cribrosa in mammalian species with good and with indifferent vision. *Br J Ophthalmol* 1956; **40**: 178–82.

57. Vurgese S, Panda-Jonas S, Jonas JB, Thompson H, Hart R. Scleral thickness in human eyes. *PLoS One* 2012; **7**: e29692.

58. Downs JC, Roberts MD, Burgoyne CF. Mechanical environment of the optic nerve head in glaucoma. *Optom Vis Sci* 2008; **85**: 425–35.

59. Quigley HA, Hohman RM, Addicks EM, Massof RW, Green WR. Morphologic changes in the lamina cribrosa correlated with neural loss in open-angle glaucoma. *Am J Ophthalmol* 1983; **95**: 673–91.

60. Hernandez MR, Andrzejewska WM, Neufeld AH. Changes in the extracellular matrix of the human optic nerve head in primary open-angle glaucoma. *Am J Ophthalmol* 1990; **109**: 180–8.

61. Crawford Downs J, Roberts MD, Sigal IA. Glaucomatous cupping of the lamina cribrosa: a review of the evidence for active progressive remodeling as a mechanism. *Exp Eye Res* 2011; **93**: 133–40.

62. Yang H, Reynaud J, Lockwood H *et al*. The connective tissue phenotype of glaucomatous cupping in the monkey eye - clinical and research implications. *Prog Retin Eye Res* 2017; **59**: 1–52.

63. Lamina cribrosa thickening in early glaucoma predicted by a microstructure motivated growth and remodeling approach. *Mech Mater* 2012; **44**: 99–109.

64. Bellezza AJ, Rintalan CJ, Thompson HW, Downs JC, Hart RT, Burgoyne CF. Deformation of the lamina cribrosa and anterior scleral canal wall in early experimental glaucoma. *Invest Ophthalmol Vis Sci* 2003; **44**: 623–37.

65. Burgoyne CF, Downs JC, Bellezza AJ, Hart RT. Three-dimensional reconstruction of normal and early glaucoma monkey optic nerve head connective tissues. *Invest Ophthalmol Vis Sci* 2004; **45**: 4388.

66. Yang H, Downs JC, Bellezza A, Thompson H, Burgoyne CF. 3-D histomorphometry of the normal and early glaucomatous monkey optic nerve head: prelaminar neural tissues and cupping. *Invest Ophthalmol Vis Sci* 2007; **48**: 5068.

67. Yang H, Downs JC, Girkin C *et al*. 3-D histomorphometry of the normal and early glaucomatous monkey optic nerve head: lamina cribrosa and peripapillary scleral position and thickness. *Invest Ophthalmol Vis Sci* 2007; **48**: 4597–607.

68. Villarruel JM, Li XQ, Bach-Holm D, Hamann S. Anterior lamina cribrosa surface position in idiopathic intracranial hypertension and glaucoma. *Eur J Ophthalmol* 2017; **27**: 55–61.

69. Fry WE. The pathology of papilledema. *Am J Ophthalmol* 1931; **14**: 874–83.

70. Lee WJ, Kim HJ, Park KH *et al*. Dynamic change in optic nerve after intracranial pressure reduction in children. *Ophthalmology* 2017; **124**: 1713–15.

71. Dellaporta A. Fundus changes in postoperative hypotony. *Am J Ophthalmol* 1955; **40**: 781–5.

72. Levy NS, Crapps EE. Displacement of optic nerve head in response to short-term intraocular pressure elevation in human eyes. *Arch Ophthalmol* 1984; **102**: 782–6.

73. Yan DB, Coloma FM, Metheetrairut A, Trope GE, Heathcote JG, Ethier CR. Deformation of the lamina cribrosa by elevated intraocular pressure. *Br J Ophthalmol* 1994; **78**: 643–8.

74. Zeimer RC, Ogura Y. The relation between glaucomatous damage and optic nerve head mechanical compliance. *Arch Ophthalmol* 1989; **107**: 1232–4.

75. Coleman AL, Quigley HA, Vitale S, Dunkelberger G. Displacement of the optic nerve head by acute changes in intraocular pressure in monkey eyes. *Ophthalmology* 1991; **98**: 35–40.

76. Fortune B, Choe TE, Reynaud J *et al*. Deformation of the rodent optic nerve head and peripapillary structures during acute intraocular pressure elevation. *Invest Ophthalmol Vis Sci* 2011; **52**: 6651.

77. Strouthidis NG, Fortune B, Yang H, Sigal IA, Burgoyne CF. Effect of acute intraocular pressure elevation on the monkey optic nerve head as detected by spectral domain optical coherence tomography. *Invest Ophthalmol Vis Sci* 2011; **52**: 9431–7.

78. Fazio MA, Johnstone JK, Smith B, Wang L, Girkin CA. Displacement of the lamina cribrosa in response to acute intraocular pressure elevation in normal individuals of African and European descent. *Invest Ophthalmol Vis Sci* 2016; **57**: 3331–9.

79. Tun TA, Thakku SG, Png O *et al*. Shape changes of the anterior lamina cribrosa in normal, ocular hypertensive, and glaucomatous eyes following acute intraocular pressure elevation. *Invest Ophthalmol Vis Sci* 2016; **57**: 4869–77.

80. Sigal IA, Flanagan JG, Tertinegg I, Ethier CR. Modeling individual-specific human optic nerve head biomechanics. Part I: IOP-induced deformations and influence of geometry. *Biomech Model Mechanobiol* 2009; **8**: 85–98.

81. Sigal IA, Yang H, Roberts MD *et al*. IOP-induced lamina Cribrosa deformation and scleral canal expansion: independent or related? *Invest Ophthalmol Vis Sci* 2011; **52**: 9023–32.

82. Roberts MD, Liang Y, Sigal IA *et al*. Correlation between local stress and strain and lamina cribrosa connective tissue volume fraction in normal monkey eyes. *Invest Ophthalmol Vis Sci* 2010; **51**: 295–307.

83. Bellezza AJ, Rintalan CJ, Thompson HW, Downs JC, Hart RT, Burgoyne CF. Anterior scleral canal geometry in pressurised (IOP 10) and non-pressurised (IOP 0) normal monkey eyes. *Br J Ophthalmol* 2003; **87**: 1284–90.

84. Furlanetto RL, Park SC, Damle UJ *et al*. Posterior displacement of the lamina Cribrosa in glaucoma: in vivo interindividual and intereye comparisons. *Invest Ophthalmol Vis Sci* 2013; **54**: 4836.

85. Lee SH, Kim T, Lee EJ, Girard JA, Mari JM. Diagnostic power of lamina cribrosa depth and curvature in glaucoma. 2017; **4**: 755–62.

86. Park SC, Brumm J, Furlanetto RL *et al*. Lamina Cribrosa depth in different stages of glaucoma. *Invest Ophthalmol Vis Sci* 2015; **56**: 2059.

87. Kim YW, Jeoung JW, Girard MJA, Mari JM, Park H. Positional and curvature difference of lamina cribrosa according to the baseline intraocular pressure in primary open-angle glaucoma: a swept-source optical coherence tomography (SS-OCT) study. *PLoS One* 2016; **11**: 1–15.

88. Thakku SG, Tham YC, Baskaran M *et al*. A global shape index to characterize anterior lamina Cribrosa morphology and its determinants in healthy Indian eyes. *Invest Ophthalmol Vis Sci* 2015; **56**: 3604.

89. Lee DS, Lee EJ, Kim TW *et al*. Influence of translaminar pressure dynamics on the position of the anterior lamina cribrosa surface. *Invest Ophthalmol Vis Sci* 2015; **56**: 2833–41.

90. Lee EJ, Kim TW, Weinreb RN, Kim H. Reversal of lamina cribrosa displacement after intraocular pressure reduction in open-angle glaucoma. *Ophthalmology* 2013; **120**: 553–9.

91. Reis ASC, O'Leary N, Stanfield MJ, Shuba LM, Nicolela MT, Chauhan BC. Laminar displacement and prelaminar tissue thickness change after glaucoma surgery imaged with optical coherence tomography. *Invest Ophthalmol Vis Sci* 2012; **53**: 5819.

92. Lee EJ, Kim TW, Weinreb RN. Reversal of lamina cribrosa displacement and thickness after trabeculectomy in glaucoma. *Ophthalmology* 2012; **119**: 1359–66.

93. Wu Z *et al*. Impact of rates of change of lamina cribrosa and optic nerve head surface depths on visual field progression in glaucoma. *Invest Ophthalmol Vis Sci* 2017; **58**: 1825.

94. Lee EJ, Kim TW, Kim M, Kim H. Influence of lamina cribrosa thickness and depth on the rate of progressive retinal nerve fiber layer thinning. *Ophthalmology* 2015; **122**: 721–9.

95. Girard MJA *et al*. In vivo 3-dimensional strain mapping of the optic nerve head following intraocular pressure lowering by trabeculectomy. *Ophthalmology* 2016; **123**: 1–11.

96. Huang W, Wang W, Zhou M *et al*. Peripapillary choroidal thickness in healthy Chinese subjects. *BMC Ophthalmol* 2013; **13**: 23.

97. Kim S-W, Oh J, Kwon S-S, Yoo J, Huh K. Comparison of choroidal thickness among patients with healthy eyes, early age-related maculopathy, neovascular age-related macular degeneration, central serous chorioretinopathy, and polypoidal choroidal vasculopathy. *Retina* 2011; **31**: 1904–11.

98. Rhodes LA, Huisingh C, Johnstone J *et al*. Variation of laminar depth in normal eyes with age and race. *Invest Ophthalmol Vis Sci* 2014; **55**: 8123–33.

99. Kim YW, Jeoung JW, Kim DW *et al*. Clinical assessment of lamina Cribrosa curvature in eyes with primary open-angle glaucoma. *PLoS One* 2016; **11**: e0150260.

100. Lee SH, Yu DA, Kim TW, Lee EJ, Girard MJA, Mari JM. Reduction of the lamina cribrosa curvature after trabeculectomy in glaucoma. *Invest Ophthalmol Vis Sci* 2016; **57**: 5006–14.

101. Chauhan BC, O'Leary N, AlMobarak FA *et al*. Enhanced detection of open-angle glaucoma with an anatomically accurate optical coherence tomography-derived neuroretinal rim parameter. *Ophthalmology* 2013; **120**: 535–43.

102. Kim M, Bojikian KD, Slabaugh MA, Ding L, Chen P. Lamina depth and thickness correlate with glaucoma severity. *Indian J Ophthalmol* 2016; **64**: 358–63.

103. Jonas JB, Hayreh SS, Yong T. Thickness of the lamina cribrosa and peripapillary sclera in rhesus monkeys with nonglaucomatous or glaucomatous optic neuropathy. *Acta Ophthalmol* 2011; **89**: e423–7.

104. You JY, Park SC, Su D, Teng CC, Liebmann JM, Ritch R. Focal lamina Cribrosa defects associated with glaucomatous rim thinning and acquired pits. *JAMA Ophthalmol* 2013; **131**: 314–20.

105. Kiumehr S *et al*. In vivo evaluation of focal lamina Cribrosa defects in glaucoma. *Arch Ophthalmol* 2012; **130**: 443–5.

106. Ohno-Matsui K, Hirakata A, Inoue M, Akiba M, Ishibashi T. Evaluation of congenital optic disc pits and optic disc Colobomas by swept-source optical coherence tomography. *Invest Ophthalmol Vis Sci* 2013; **54**: 7769.

107. Tatham AJ, Miki A, Weinreb RN, Zangwill LM, Medeiros FA. Defects of the lamina Cribrosa in eyes with localized retinal nerve fiber layer loss. *Ophthalmology* 2014; **121**: 110–18.

108. Faridi OS, Park SC, Kabadi R *et al*. Effect of focal lamina Cribrosa defect on glaucomatous visual field progression. *Ophthalmology* 2014; **121**: 1524–30.

109. Takayama K, Hangai M, Kimura Y *et al*. Three-dimensional imaging of lamina cribrosa defects in glaucoma using swept-source optical coherence tomography. *Invest Ophthalmol Vis Sci* 2013; **54**: 4798.

110. Park SC, Hsu AT, Su D *et al*. Factors associated with focal lamina cribrosa defects in glaucoma. *Invest Ophthalmology Vis Sci* 2013; **54**: 8401.

111. Lee EJ, Kim TW, Kim M, Girard MJA, Mari JM, Weinreb RN. Recent structural alteration of the peripheral lamina cribrosa near the location of disc hemorrhage in glaucoma. *Invest Ophthalmol Vis Sci* 2014; **55**: 2805.

112. Kim YK, Park K. Lamina cribrosa defects in eyes with glaucomatous disc haemorrhage. *Acta Ophthalmol* 2016; **94**: e468–73.

113. Airaksinen PJ, Mustonen E, Alanko HI. Optic disc haemorrhages precede retinal nerve fibre layer defects in ocular hypertension. *Acta Ophthalmol* 1981; **59**: 627–41.

114. Demer JL. Optic nerve sheath as a novel mechanical load on the globe in ocular duction. *Invest Ophthalmol Vis Sci* 2016; **57**: 1826–38.

115. Wang X, Rumpel H, Lim WEH *et al.* Finite element analysis predicts large optic nerve head strains during horizontal eye movements. *Invest Ophthalmol Vis Sci* 2016; **57**: 2452.

116. Wang X, Beotra MR, Tun TA *et al.* In vivo 3-dimensional strain mapping confirms large optic nerve head deformations following horizontal eye movements. *Invest Ophthalmol Vis Sci* 2016; **57**: 5825.

117. Suh SY, Le A, Shin A, Park J, Demer JL. Progressive deformation of the optic nerve head and peripapillary structures by graded horizontal duction. *Invest Ophthalmol Vis Sci* 2017; **58**: 5015–21.

118. Sibony PA. Gaze evoked deformations of the peripapillary retina in papilledema and ischemic optic neuropathy. *Invest Ophthalmol Vis Sci* 2016; **57**: 4979.

119. Leydhecker W, Akiyama K, Neumann HG. Intraocular pressure in normal human eyes. *Klin Monbl Augenheilkd Augenarztl Fortbild* 1958; **133**: 662–70.

120. O'Hara KE, Schmoll T, Vass C, Leitgeb RA. Measuring pulse-induced natural relative motions within human ocular tissue *in vivo* using phase-sensitive optical coherence tomography. *J Biomed Opt* 2013; **18**: 121506.

121. Dragostinoff N, Werkmeister RM, Klaizer J, Gröschl M, Schmetterer L. Time course and topographic distribution of ocular fundus pulsation measured by low-coherence tissue interferometry. *J Biomed Opt* 2013; **18**: 121502.

122. Ang M, Konstantopoulos A, Goh G *et al.* Evaluation of a micro-optical coherence tomography for the corneal endothelium in an animal model. *Sci Rep* 2016; **6**: 29769.